www.nature.com/scientificreports

SCIENTIFIC REPORTS

OPEN

Received: 17 June 2016
Accepted: 23 September 2016
Published: 07 October 2016

Ultrafast spin dynamics and switching via spin transfer torque in antiferromagnets with weak ferromagnetism

Tae Heon Kim[1,2], Peter Grünberg[2], Song Hee Han[3] & Beongki Cho[1,2]

The spin-torque driven dynamics of antiferromagnets with Dzyaloshinskii-Moriya interaction (DMI) were investigated based on the Landau-Lifshitz-Gilbert-Slonczewski equation with antiferromagnetic and ferromagnetic order parameters (*l* and *m*, respectively). We demonstrate that antiferromagnets including DMI can be described by a 2-dimensional pendulum model of *l*. Because *m* is coupled with *l*, together with DMI and exchange energy, close examination of *m* provides fundamental understanding of its dynamics in linear and nonlinear regimes. Furthermore, we discuss magnetization reversal as a function of DMI and anisotropy energy induced by a spin current pulse.

Since the first discovery of sub-picosecond demagnetization of ferromagnetic nickel film using femtosecond infrared lasers, ultrafast manipulation of magnetization has raised much interest in terms of both condensed matter physics and applications in information storage devices[1]. Together with the development of femtosecond lasers, a considerable number of research studies have been conducted to explore the microscopic dynamics experimentally as well as theoretically for various magnetic systems[2–13].

The antiferromagnet (AF) system is a promising structure for ultrafast processes because it has a relatively strong exchange interaction that shifts the precession frequency into the terahertz range. The AF system can be excited or switched at picosecond timescales (significantly faster than ferromagnetic precession[14–17]), and AF switching through current-induced spin transfer torque has been recently measured electrically[18].

AF systems with weak ferromagnetism (AWF) might be useful for memory devices because of their weak ferromagnetism and selectively controllable excitation modes[19]. The weak ferromagnetism is associated with broken inversion symmetry in the material and is independent of any ferromagnetic impurities[20]. This type of magnetism has been studied experimentally in the rare earth orthoferrites[21–26] and rhombohedral antiferromagnet $FeBO_3$[27,28] by many research groups. However, analytical approaches to describe AWF dynamics are rare except for AF cases[15,29].

This paper shows that AWF dynamics is governed by the classical pendulum equations on the antiferromagnetic order parameter ($\boldsymbol{l}$), similar to the simple AF case[14]. We demonstrate quantitatively that the occurrence of the second harmonic of the ferromagnetic order parameter ($\boldsymbol{m}$) is direct evidence for a nonlinear regime, including resonant frequency softening[30], and that the ellipticity of the precessional motion of $\boldsymbol{m}$ determines the Dzyaloshinskii-Moriya interaction (DMI) energy. Additionally, we propose that sub-lattice dynamics ($\boldsymbol{s}_1$, $\boldsymbol{s}_2$) can be revealed experimentally. We discuss switching efficiency as a function of anisotropy, DMI energy and damping constant (α) using spin current pulse with various durations and densities.

Theory

AWF dynamics. Figure 1 shows AWF static and dynamic configurations based on two sub-lattice models below the Néel temperature[31]. Antiferromagnetically coupled spins lie along the x-axis because the anisotropy of the spins occurs along the uniaxial direction, with the magnetic easy axis parallel to x-axis, and the spins are tilted along the z-axis due to the DMI vector, $-D_y\hat{y}$, as shown in Fig. 1(a). The DMI produces two resonant modes, called the Sigma mode and the Gamma mode (S- and G-mode, respectively)[19].

[1]School of Materials Science and Engineering, Gwangju Institute of Science and Technology (GIST), Gwangju 61005, Republic of Korea. [2]Grünberg Center for Magnetic Nanomaterials, Gwangju Institute of Science and Technology (GIST), Gwangju 61005, Republic of Korea. [3]Division of Navigation Science, Mokpo National University, Mokpo 58628, Republic of Korea. Correspondence and requests for materials should be addressed to B.C. (email: chobk@gist.ac.kr)

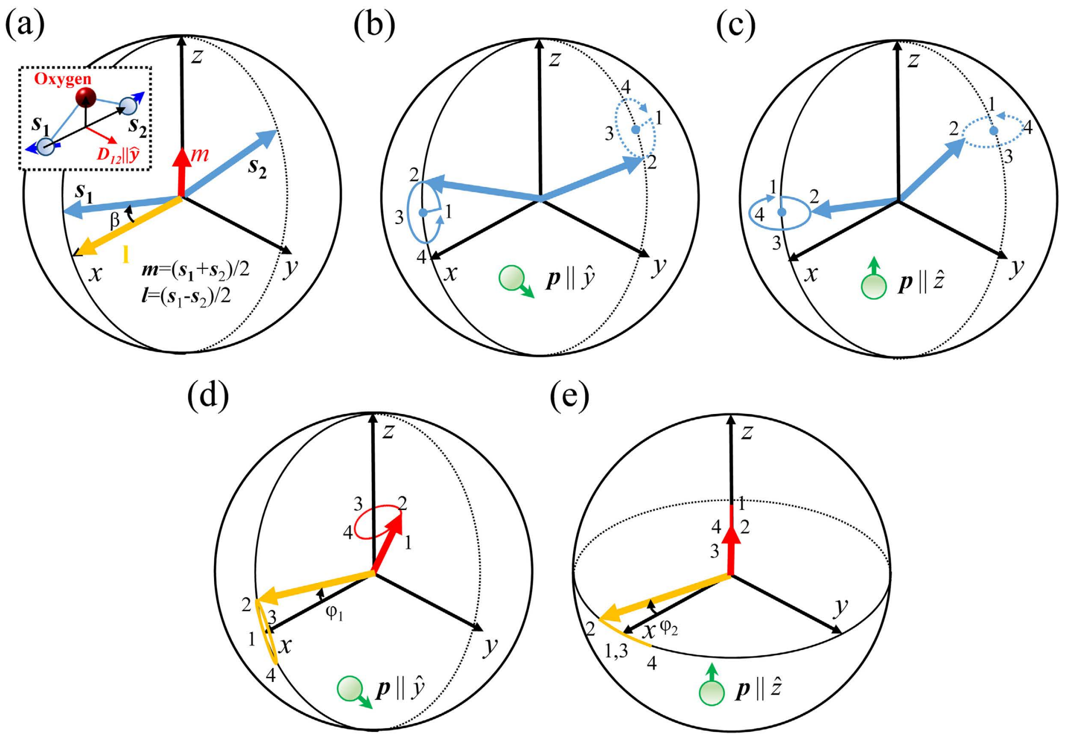

Figure 1. (**a**) Schematic diagram for an antiferromagnet with Dzyaloshinskii-Moriya interaction at $T < T_N$. The ferromagnetic order parameter, *m*, and the antiferromagnetic order parameter, *l*, are defined as $(s_1 + s_2)/2$ and $(s_1 - s_2)/2$, respectively. *m* is exaggerated compared to *l*. Inset shows the DM interaction mechanism between the sub-lattices and oxygen. Two resonant modes are selectively excited depending on the injected spin polarization: Sigma mode in $p||\hat{y}$ (**b**) and Gamma mode in $p||\hat{z}$ (**c**). (**d,e**) are reproductions of (**b,c**), respectively, in terms of *l* and *m*.

Landau-Lifshitz-Gilbert-Slonczewski equation. To better understand the kinetics of AWF, the total energy based on two sub-lattices with $i = 1, 2$ is expressed as

$$U = Js_i \cdot s_{3-i} + D \cdot (s_i \times s_{3-i}) + K_x[(s_{i,x})^2 + (s_{3-i,x})^2] + K_z[(s_{i,z})^2 + (s_{3-i,z})^2], \tag{1}$$

where the normalized magnetization, $\mathbf{s}_i = \mathbf{S}_i/S_0$ with $S_0 = |\mathbf{S}_i|$ is dimensionless, and $\hbar$ is the reduced Plank constant. The first term is related to the exchange energy, where *J* is the nearest-neighbor symmetric exchange constant, with the positive sign accounting for AF coupling. The second term describes Dzyaloshinskii-Moriya (DM) energy, where the DM vector, $\boldsymbol{D}$, is $-D_y\hat{y}$, $D_y > 0$, and its magnitude is relatively weak. The third and fourth terms are anisotropy energies where anisotropy constants are $K_x > 0$ and $K_z < 0$, indicating magnetic in-plane and out-of-plane anisotropy, respectively. These energy combinations cause the anti-parallel spins to be tilted slightly along the *z*-axis. The dynamics can be described by the coupled Landau-Lifshitz-Gilbert-Slonczewski equation of motion:

$$\dot{s}_i = [Js_i \times s_{3-i} + (-1)^{i+1} s_i \cdot (D \times s_{3-i}) + K_x\hat{x} \times s_i + K_z\hat{z} \times s_i]/\hbar + \alpha s_i \times \dot{s}_i + \Omega s_i \times (s_i \times p), \tag{2}$$

The fifth term is phenomenological damping, which is characterized by the Gilbert damping constant (α). The final term is the Slonczewski-type spin transfer torque (STT), where $\boldsymbol{p}$ is the unit vector of spin polarization, and Ω is the STT strength with angular frequency unit, defined as $\varepsilon\hbar\gamma J_s/(2VS_0 e)$, which is proportional to the spin current density, J_s, where ε and *V* are the scattering efficiency and volume of AWF region, respectively[14,29,32].

We use staggered magnetization, $\boldsymbol{l} = (\boldsymbol{s}_1 - \boldsymbol{s}_2)/2$, and weak magnetization, $\boldsymbol{m} = (\boldsymbol{s}_1 + \boldsymbol{s}_2)/2$, so that Eq. (2) becomes

$$\dot{m} = [-D \times (m \times l) + K_x\hat{x} \times (m_x l + l_x m) + K_z\hat{z} \times (m_z l + l_z m)]/\hbar + Damping + STT, \tag{3}$$

$$\dot{l} = [2J(l \times m) + K_x\hat{x} \times (m_x l + l_x m) + K_z\hat{z} \times (m_z l + l_z m)]/\hbar + Damping + STT, \tag{4}$$

where *Damping* and *STT* are $\boldsymbol{\alpha}(\boldsymbol{m} \times \boldsymbol{l} + \boldsymbol{l} \times \boldsymbol{m})$ and $\boldsymbol{\Omega}[\boldsymbol{m} \times (\boldsymbol{l} \times \boldsymbol{p}) + \boldsymbol{l} \times (\boldsymbol{m} \times \boldsymbol{p})]$, respectively. Equations (3) and (4) are constrained by

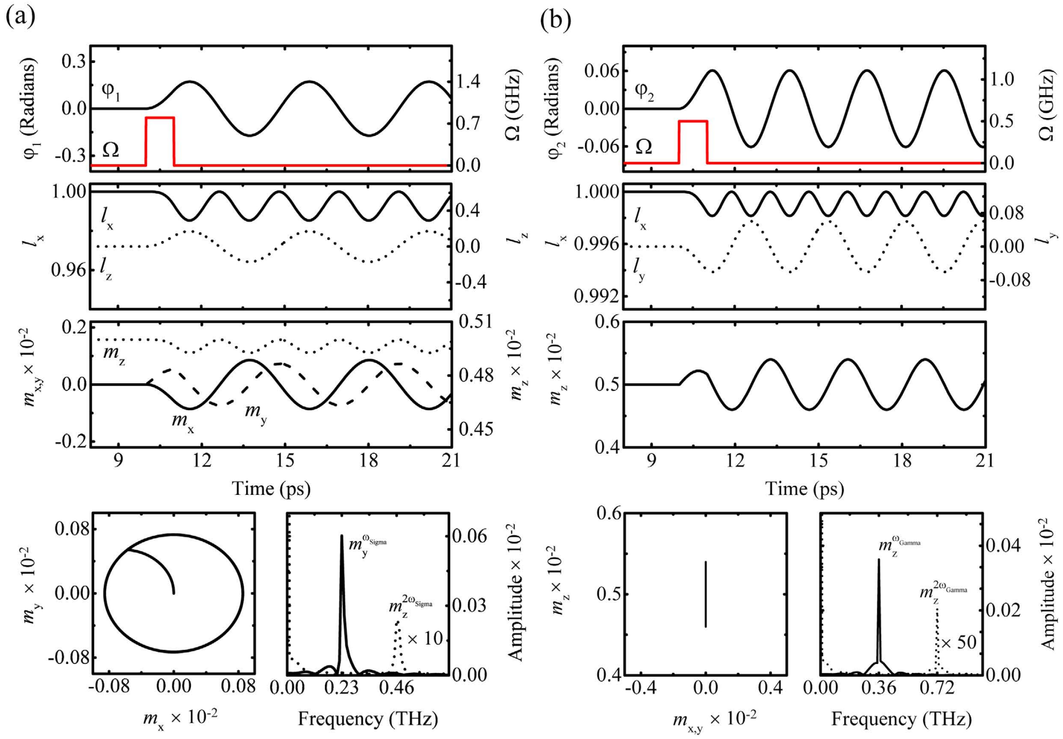

Figure 2. Excitation modes when (**a**) $\boldsymbol{p}||\hat{y}$ and $\Omega = 0.8$ GHz and (**d**) $\boldsymbol{p}||\hat{z}$ and $\Omega = 0.5$ GHz. Spin trajectories (left) and spectra (right) are shown in fourth row. In both cases, the pulse duration (τ) is 1 ps and the Gilbert damping constant is 0 (see Supplementary Movie 1 and 2).

$$\begin{aligned} &m \cdot l = 0, \\ &m^2 + l^2 = 1, \\ &|m| \ll |l|, \\ &l^2 \sim 1 \rightarrow l \cdot \dot{l} \sim 0. \end{aligned} \tag{5}$$

Consider the S-mode excited by spin current with polarization, $\boldsymbol{p}||\hat{y}$. When the STT turns on, $\boldsymbol{s}_1$ and $\boldsymbol{s}_2$ are dragged slightly toward the y-axis by the exchange coupling between the conduction electrons and the magnetic moments, as shown in Fig. 1(b). Consequently, as m_y increases in magnitude, $\boldsymbol{l}$ is moved away from its equilibrium position. After the STT turns off, $\boldsymbol{l}$ and $\boldsymbol{m}$ are subject to an internal magnetic field torque, and $\boldsymbol{m}$ precesses on the xy-plane and fluctuates along the z-axis, as shown in Fig. 1(d). (In a simple AF, only m_y fluctuation is shown[14,17,29].) This is ascribed to the DMI, coupled with m_x and m_z, which causes elliptical polarization of precessional motion of $\boldsymbol{m}$, as shown in Fig. 1(d). The details are discussed below, in conjunction with the second harmonic oscillation of m_z.

Because the l_y component is much smaller than l_x and l_z, the dynamics of $\boldsymbol{l}$ can be regarded as approximately 2-dimensional (2D) pendulum motion oscillating with angle φ_1 on the xz-plane (see Supplementary information). Therefore, we expand Eqs (3) and (4) by using the effective vectors (l_x, 0, l_z) and (0, m_y, 0), and take the cross product of $\boldsymbol{l}$ on Eq. (4) to extract only $\boldsymbol{m}$,

$$\frac{\dot{l} \times l}{2J/\hbar} \sim \left(\frac{-D_y l_z}{2J}, m_y, \frac{D_y l_x}{2J}\right) = m, \tag{6}$$

$$m_y \sim \frac{-l_z \dot{l}_x + l_x \dot{l}_z}{2J/\hbar}, \tag{7}$$

where the equations are simplified by employing Eq. (5) and ignoring terms coupled with anisotropy energy because $|K_x|$ and $|K_z| \ll D_y$ and J. Substituting Eq. (7) into Eq. (3), we have the 2D pendulum equations,

$$\ddot{\varphi}_1 + \dot{\varphi}_1 2\alpha J/\hbar + \sin[2\varphi_1]\omega_{\text{Sigma}}^2/2 = 2J\Omega p_{\text{y}}/\hbar \text{ from } (l_x, l_z) = (\cos[\varphi_1], \sin[\varphi_1]), \tag{8}$$

where $\omega_{\text{Sigma}}^2 = 2J(K_x - K_z)/\hbar^2$.

In G-mode, $\boldsymbol{p}||\hat{z}$; thus, $\boldsymbol{s}_1$ and $\boldsymbol{s}_2$ are dragged slightly toward the z-axis, as shown in Fig. 1(c). As m_z increases in magnitude, with m_x and m_y remaining zero, $\boldsymbol{l}$ is moved away from the equilibrium position (see Supplementary

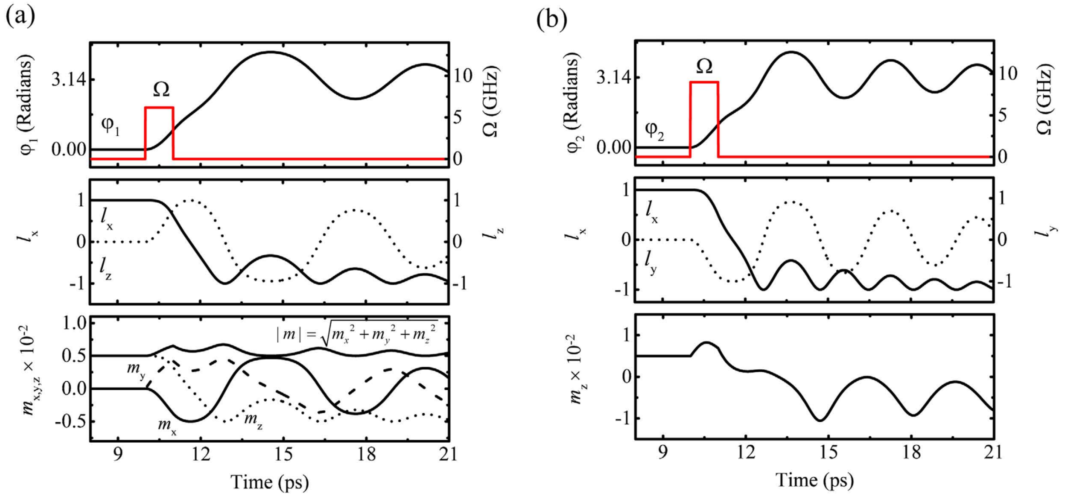

Figure 3. Magnetization switching when (**a**) $\boldsymbol{p}||\hat{y}$ and $\Omega = 6.2$ GHz and (**b**) $\boldsymbol{p}||\hat{z}$ and $\Omega = 9$ GHz. In both cases, the pulse duration (τ) is 1 ps and the Gilbert damping constant is 0.0005 (see Supplementary Movie 3 and 4).

information). After STT turns off, m_z shows only fluctuation motion and $\boldsymbol{l}$ oscillates on the *xy*-plane, as shown in Fig. 1(e). The methodology in S-mode is used again, so that

$$\frac{\dot{l} \times l + l_x \cdot D_y/\hbar}{2J/\hbar} \sim (0,\, 0,\, m_z) = m \tag{9}$$

$$m_z \sim \frac{-l_x\dot{l}_y + l_y\dot{l}_x + l_x \cdot D_y/\hbar}{2J/\hbar}. \tag{10}$$

Substituting Eq. (9) into Eq. (3), the 2D pendulum equation becomes

$$\ddot{\varphi}_2 + \dot{\varphi}_2 2\alpha J/\hbar + \sin[2\varphi_2]\omega_{\text{Gamma}}^2/2 = 2J\Omega p_z/\hbar \text{ from } (l_{\text{x}},\, l_{\text{y}}) = (\cos[\varphi_2],\, \sin[\varphi_2]), \tag{11}$$

where $\omega_{\text{Gamma}}^2 = 2J(K_x + D_y \tan[\beta])/\hbar^2$, with spin canting angle β in equilibrium (l and $l_z = 0$) because $\tan[\beta] = m_z/l_x = D_y/(2J)$. These outcomes confirm White *et al.*[19].

Results and Discussion

Ultrafast dynamics in the terahertz regime. We introduce the DMI or antisymmetric super-exchange interaction from the triangle spanned among three ions (magnetic ions and oxygen ion). Such an interaction was discovered in the interface between AF and ferromagnet[33], and between AF and ferrimagnet superlattices[34], as well as bulk crystals[20–26]. Here, we suppose a two-layer system consisting of two antiferromagnetic oxides, where the interaction between two magnetic ions arranged along the *x*-axis, and the oxygen ion, shifted slightly to the *z*-axis, gives rise to DM vector,$-|D_y|\hat{y}$, as shown in the inset of Fig. 1(a). Because the magnetic easy axis is the *x*-axis, sub-lattice spins are canted toward the *z*-axis. Additionally, we assume that the magnetic unit cell exhibits weak ferromagnetism, as in the case of rare earth ferrite, ReFeO_3 single crystal (Re: Er, Tm, and Y, etc). The parameters chosen were $J = 113.5$ meV, $K_x = 4.14\,\mu$eV, $K_z = 0$, and $D_y = 0.01J$ so that spin precession motion is in the terahertz frequency range. To inject spin current into AWF, we exploit the spin hall effect in Pt with strong spin-orbit coupling. Figure 2(a,b) show S-mode and G-mode in AWF (see Supplementary Movie 1 & 2). Moreover, we checked that our analytical results are validated by numerical calculations based on Eq. (1) (see Supplementary Figure 2 and 3). However, for stronger DM energy, we found that the analytical solution deviates from the numerical one because the approximation ($|m| \ll |l|,\;\; l^2 \sim 1 \rightarrow l \cdot \dot{l} \sim 0.$) is no longer valid. (see Supplementary information).

Second harmonic oscillation of *M*$_z$ as a nonlinear effect. S- and G-mode dynamics have common characteristic motion: second harmonic oscillations along the *z*-axis. According to Eqs (6) and (9), $m_z^{2\omega_{\text{Sigma}}}$ and $m_z^{2\omega\ \text{Gamma}}$ are both responsible for the nonlinearity of l_x, together with the resonant frequency softening[30]. For example, φ_1(t) is sinusoidal in $\Omega = 0.8$ GHz; as a results, $m_z = l_x \cdot D_y/\hbar \sim \cos[\varphi_1(t)] = \cos[A\sin[\omega_{\text{Sigma}}t]]$ is replaced with $\sim(1 - A^2/4) - A^2\cos[2\omega_{\text{Sigma}}t]/4$ by its first order Taylor expansion. Likewise, $m_z^{2\omega_{\text{Sigma}}}$and $m_z^{2\omega_{\text{Gamma}}}$are shown in Fig. 2(a,b), fourth row, right.

Determination of DMI strength. The DMI strength can be obtained by examining the first harmonic precession on the *xy*-plane in the S-mode, $m_{xy}^{\omega_{\text{Sigma}}} = (m_x\hat{x} + m_y\hat{y})\sin\;[\omega_{\text{Sigma}}t]$. Using Eqs (6) and (7), the ellipticity, ε is calculated as $m_y(t)/m_x(t) = [-2J/(D_y l_z)]\;\hbar(-l_z\dot{l}_x + l_x\dot{l}_z)/(2J)] = A\hbar\omega_{\text{Sigma}}\cos[\omega_{\text{Sigma}}t]/$

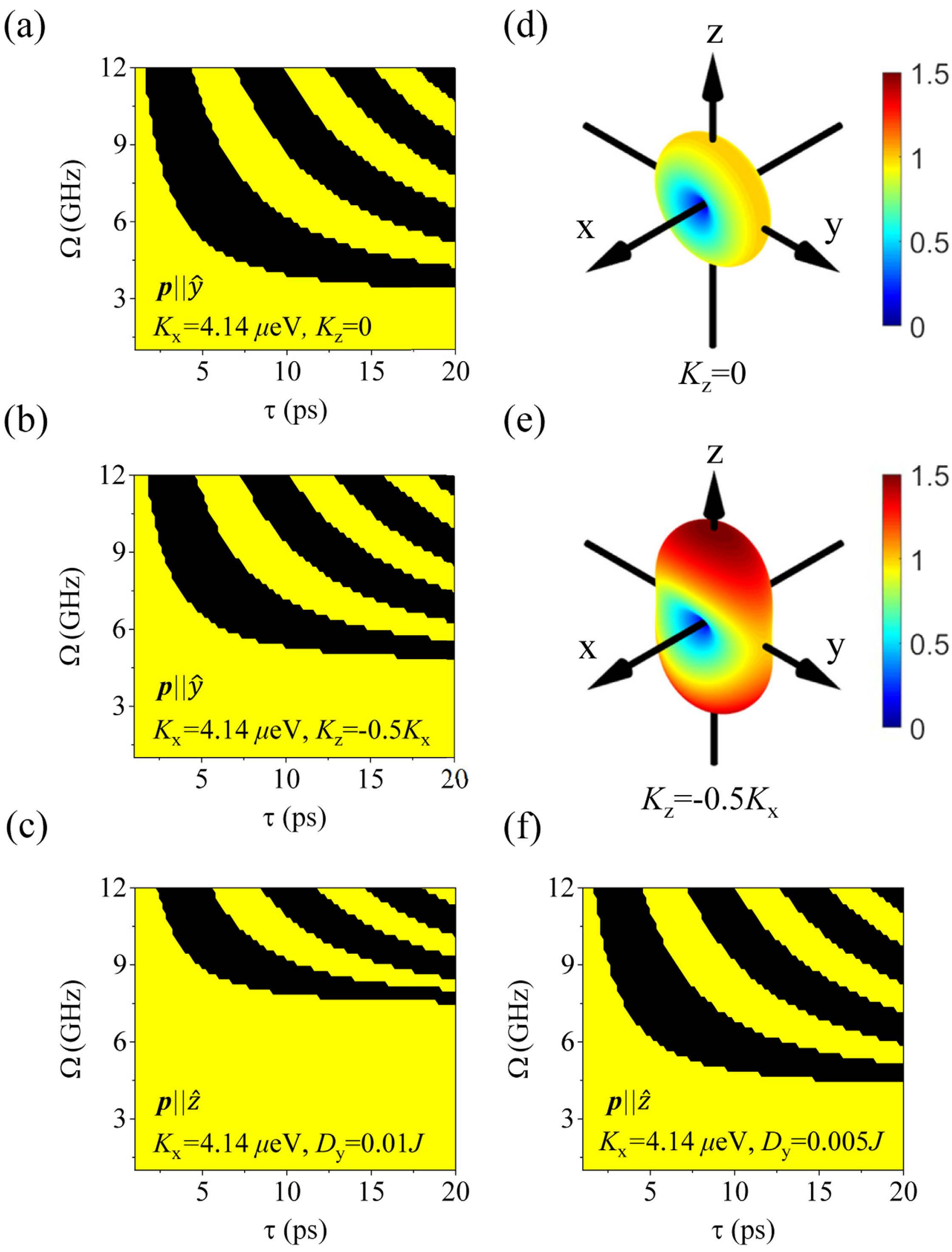

Figure 4. (**a–c,f**) Periodic patterns of terminal phase of l_x for various conditions of K_x, K_z, D_y, and $\boldsymbol{p}$ in the Ω versus τ plot after excitation by a pulsed spin current. From left down to right up, the terminal phases of l_x are indicated by $n\pi$, $n = 0, 1, 2, \ldots$ (even = yellow, odd = black), $\alpha = 0.01$. (**d–e**) Potential energy distribution with $K_z = 0$, $K_z = -0.5\,K_x$, and $K_x = 4.14\,\mu$eV.

($D_y\sin[A\sin[\omega_{\text{Sigma}}t]]$). If we assume A is small enough, $\varepsilon \sim \hbar\omega_{\text{Sigma}}/(D_y \tan[\omega_{\text{Sigma}}t])$. For example, $\varepsilon = |m_y/m_x| \sim 0.85$ is constant within a few percent with $\hbar\omega_{\text{Sigma}}/D_y = 0.953/11.35 \sim 0.84$, as shown in Fig. 2(a), fourth row, left. Experimentally, the precessional polarization in S-mode can be measured using optical tools: terahertz time domain spectroscopy[23–28,30], or time resolved magneto optical Kerr/Faraday rotation[16,21,22].

s_1 and s_2 deduced from m and l. Once the DMI strength is determined, J is easily estimated by using well-known antisymmetric exchange model, $M_s \sim M_0D_y/(2J)$[35], where saturation magnetization, M_s can be measured by using a conventional sample vibrating magnetometer. M_0 is the number of magnetic ions per volume or mole. Conventional time domain terahertz spectroscopy (or time resolved magneto optical Kerr/Faraday rotation technique) can be used to observe $\boldsymbol{m}(t)$. From the Fourier transform of $m_x(t)$ (or $m_y(t)$) and $m_z(t)$, the resonant frequencies (and thereby K_x and K_z) are obtained. As $\boldsymbol{m}$, D, and J are determined, $\boldsymbol{l}$ could be estimated using Eqs (6) and (9). For example, in S-mode, l_z and l_x can be deduced from m_x and m_z using Eqs (5) and (6). In G-mode, l_x and l_z can be estimated using Eqs (8) and (9) and the spectral amplitude and phase information. The resulting $\boldsymbol{s}_1$ and $\boldsymbol{s}_2$ are shown in Fig. 1(b,c). In contrast, l_x is not extractable in simple AF because of the lack of DMI[14].

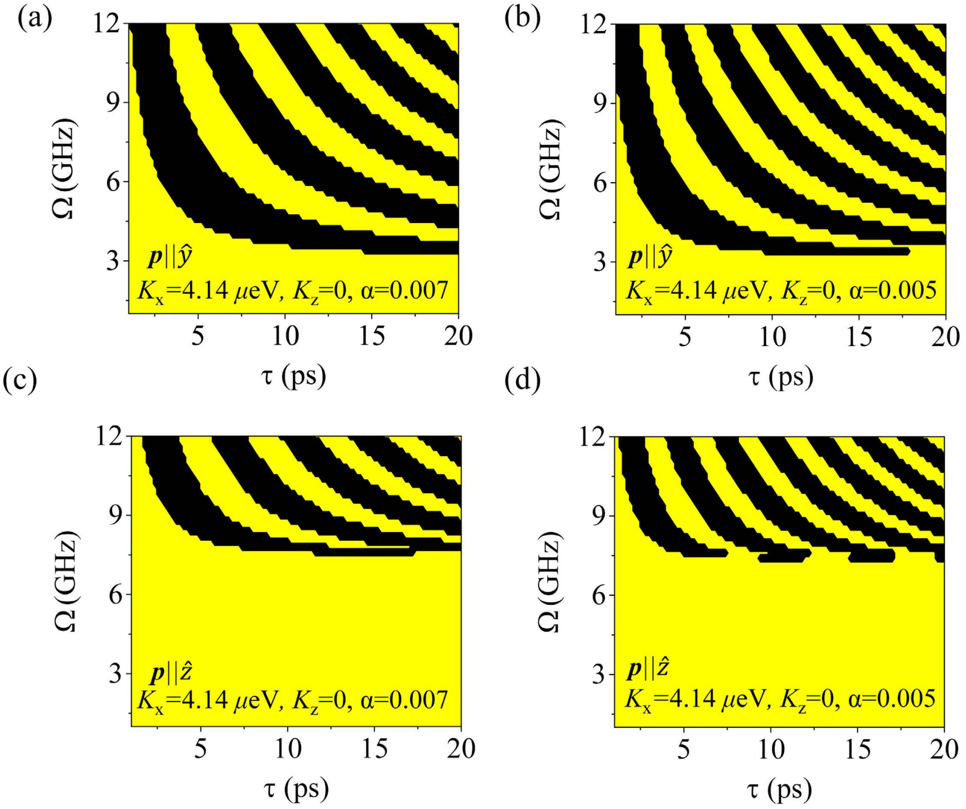

Figure 5. Periodic patterns of the terminal phase of l_x for different damping constants for S- and G-mode: (**a**,**c**) the damping constant is 0.007, and (**b**,**d**) the damping constant is 0.005. In these cases, the pulse duration is 1 ps.

Switching mechanism and efficiency. Figure 3(a,b) show the switching process for S-mode and G-mode, respectively (see Supplementary Movie 3 and 4). In S-mode, $|\boldsymbol{m}|$, defined as $\sqrt{m_x^2 + m_y^2 + m_z^2}$, (or m_z in G-mode), increases in magnitude less than 1% for $|\boldsymbol{l}_{\max}| \sim 1$ with the spin current pulse. Additional canting is converted into kinetic energy, and if the kinetic energy exceeds the maximum potential energy, spin reversal occurs after the pulse has been turned off. This is inertia-driven switching[17], and the switching is identically applied in G-mode.

Because either ω_{Sigma} or ω_{Gamma} could be manipulated by K_z or D_y, switching efficiency should be considered for these parameters. Figure 4 shows the periodic patterns for the terminal phase of l_x for various values of K_x and D_y after excitation by spin current pulses for several values of τ, Ω and $\boldsymbol{p}$. From left down to right up, terminal phases of l_x are indicated by $n\pi$, $n = 0, 1, 2$.

When the potential barrier increases from $K_z = 0$ in Fig. 4(d) to $K_z = -0.5|K_x|$ in Fig. 4(e), $\boldsymbol{l}$ in S-mode must overcome the higher potential barrier on the xz-plane. Thus, phases of l_x are shifted upward in Fig. 4(b), compared to Fig. 4(a). Another factor to modify the switching efficiency is the DMI strength in G-mode, where K_z does not play a role in the control of the energy barrier on the xy-plane because the energy barrier on the xz-plane is controllable by K_z. When $D_y = 0.01\,J$ in Fig. 4(c), the pendulum system energy is higher than that of $D_y = 0.005\,J$ in Fig. 4(f), and the first switching demands higher STT strength. Experimentally, magnetic materials have temperature dependence on anisotropy energies or thickness dependence on D_y[33,36]. Additionally, the interface engineering is used to change DMI strength[37]. Applying these properties, one can expect to switch magnetization under optimal conditions. In particular, AWF systems, which have anisotropy with two easy-axes (K_x and $K_z > 0$), would undergo switching at a lower critical STT strength (Ω_c) in S-mode, because K_z lowers the switching barrier. Finally, we checked the α dependence. When the pulse duration (τ) is short, the damping effect obviously lowers Ω_c: For example, $\Omega_c = 4.4\,\mathrm{GHz}$, $\tau = 5\,\mathrm{ps}$ for $\alpha = 0.007$ and $\Omega_c = 3.8\,\mathrm{GHz}$, $\tau = 5\,\mathrm{ps}$ for $\alpha = 0.005$ in Fig. 5(a,b). In general, as α becomes smaller, the periodic patterns become narrower[14]. In particular, in short τ, the slope of the phase boundary is steep and dependent on α; thus, one might doubt its stable functionality as a device. In long τ, Ω_c is much reduced and finally become minimized, but its magnitude is not further reduced for variation of α.

Conclusion

In summary, we investigated the process of precession motion in antiferromagnets with weak ferromagnetism through spin transfer torque. Although DMI splits the AF resonant mode into S- and G-modes, the modes are also be interpreted as pendulum models on $\boldsymbol{l}$. Because $\boldsymbol{l}$ and DMI energy are coupled and independently extractable through measurement of $\boldsymbol{m}$, dynamic analysis of $\boldsymbol{m}$ provides fundamental understanding of sub-lattice dynamics, as shown in Fig. 1(b,c). Adjustment of appropriate parameters, such as the anisotropy barrier and DMI strength, provide more efficient magnetization reversal.

References

1. Beaurepaire, E., Merle, J.-C., Daunois, A. & Bigot, J.-Y. Ultrafast spin dynamics in ferromagnetic Nickel. *Phys. Rev. Lett.* **76,** 4250 (1996).
2. Kirilyuk, A., Kimel, A. V. & Rasing, Th. Ultrafast optical manipulation of magnetic order. *Rev. Mod. Phys.* **82,** 2731–2784 (2010).
3. Stanciu, C. D. *et al.* All-optical magnetic recording with circularly polarized light. *Phys. Rev. Lett.* **99,** 047601 (2007).
4. Koopmans, B., van Kampen, M., Kohlhepp, J. T. & de Jonge, W. J. M. Ultrafast magneto-optics in nickel: Magnetism or Optics? *Phys. Rev. Lett.* **85,** 844–847 (2000).
5. Guidoni, L., Beaurepaire, E. & Bigot, J.-Y. Magneto-optics in the ultrafast regime: Thermalization of Spin Populations in Ferromagnetic Films. *Phys. Rev. Lett.* **89,** 017401 (2002).
6. Zhang, G. P., Hubner, W., Lefkidis, G., Bai, Y. & George, T. F. Paradigm of the time-resolved magneto-optical Kerr effect for femtosecond magnetism. *Nature Phys*. **5,** 499–502 (2009).
7. Carva, K., Battiatio, M. & Oppeneer, P. M. Is the controversy over femtosecond magneto-optics really solved? *Nature Phys*. **7,** 665–666 (2011).
8. Malinowski, G. *et al.* Control of speed and efficiency of ultrafast demagnetization by direct transfer of spin angular momentum. *Nature Phys*. **4,** 855–858 (2008).
9. Bigot, J.-Y., Vomir, M. & Beaurepaire, E. Coherent ultrafast magnetism induced by femtosecond laser pulses. *Nature Phys*. **5,** 515–520 (2009).
10. Zhang, G. P., Bai, Y. & George, T. F. Energy- and crystal momentum-resolved study of laser-induced femtosecond magnetism. *Phys. Rev. B* **80,** 214415 (2009).
11. Koopmans, B. *et al.* Magnetization dynamics: Ferromagnets stirred up. *Nature Mater*. **9,** 259–265 (2010).
12. Battiato, M., Carva, K. & Oppeneer, P. M. Superdiffusive spin transport as a mechanism of ultrafast demagnetization. *Phys. Rev. Lett.* **105,** 027203 (2010).
13. Fähnle, M. & Illg, C. Electron theory of fast and ultrafast dissipative magnetization dynamics. *J. Phys. Condens. Matter* **23,** 493201 (2011).
14. Cheng, R., Daniels, M. W., Zhu, J. G. & Xiao, D. Ultrafast switching of antiferromagnets via spin-transfer torque. *Phys. Rev. B* **91,** 064423 (2015).
15. Cheng, R., Xiao, J., Niu, Q. & Brataas, A. Spin pumping and spin-transfer torques in Antiferromagnets. *Phys. Rev. Lett.* **113,** 057601 (2014).
16. Kampfrath, T. *et al.* Coherent terahertz control of antiferromagnetic spin waves. *Nat. Photonics* **5,** 31 (2011).
17. Wienholdt, S., Hinzke, D. & Nowak, U. THz switching of antiferromagnets and ferrimagnets. *Phys. Rev. Lett.* **108,** 247207 (2012).
18. Wadley, P. *et al.* Electrical switching of an antiferromagnet. *Science* **351,** 587 (2016)
19. White, R. M., Nemanich, R. J. & Herring, C. Light scattering from magnetic excitations in orthoferrites. *Phys. Rev. B* **25,** 1822 (1982).
20. Dzyaloshinsky, I. A thermodynamic theory of weak ferromagnetism of antiferromagnetics. *J. Phys. Chem. Solids* **4,** 241–255 (1958).
21. Kimel, A. V. *et al.* Ultrafast non-thermal control of magnetization by instantaneous photomagnetic pulses. *Nature* **435,** 655 (2005).
22. Kimel, A. V. *et al.* Inertia-driven spin switching in antiferromagnets. *Nature Phys*. **5,** 727 (2009).
23. Kim, T. H. *et al.* Coherently controlled spin precession in canted antiferromagnetic $YFeO_3$ using terahertz magnetic field. *Appl. Phys. Express* **7,** 093007 (2014).
24. Mikhaylovskiy, R. V. *et al.* Terahertz emission spectroscopy of laser-induced spin dynamics in TmFeO3 and ErFeO3 orthoferrites. *Phys. Rev. B* **90,** 184405 (2014).
25. Kim, T. H. *et al.* Magnetization states of canted antiferromagnetic YFeO3 investigated by terahertz time-domain spectroscopy. *J. Appl. Phys.* **118.** 233101 (2015).
26. Mikhaylovskiy, R. V. *et al.* Terahertz magnetization dynamics induced by femtosecond resonant pumping of Dy^{3+} subsystem in the multisublattice antiferromagnet $DyFeO_3$. *Phys. Rev. B* **92,** 094437 (2015).
27. Mikhaylovskiy, R. V. *et al.* Ultrafast optical modification of exchange interactions in iron oxides. *Nat. Commun.* **6,** 8190 (2015).
28. Huisman, T. J.,Mikhaylovskiy, R. V., Tsukamoto, A., Rasing, Th. & Kimel, A. V. Simultaneous measurements of terahertz emission and magneto-optical Kerr effect for resolving ultrafast laser-induced demagnetization dynamics. *Phys. Rev. B* **92,** 104419 (2015).
29. Gomonay, H. V. & Loktev, V. M. Spin transfer and current-induced switching in antiferromagnets. *Phys. Rev. B* **81,** 144427 (2010).
30. Mukai, Y., Hirori, H., Yamamoto, T., Kageyama, H. & Tanaka, K. Nonlinear magnetization dynamics of antiferromagnetic spin resonance induced by intense terahertz magnetic field. *New J. Phys*. **18** 013045 (2016).
31. Kocharyan, K. N., Martirosyan, R. M., Prpryan, V. G. & Sarkisyan, E. L. Faraday effect in yttrium orthoferrite in the “low-frequency” antiferromagnetic resonance region. *Sov. Phys. JETP* **59,** 373 (1984).
32. Slonczewski, J. C. Current-driven excitation of magnetic multilayers. *J. Magn. Magn. Mater.* **159,** 1 (1996).
33. Dong *et al.* Exchange Bias Driven by the Dzyaloshinskii-Moriya Interaction and Ferroelectric Polarization at G-Type Antiferromagnetic Perovskite Interfaces. *Phys. Rev, Lett.* **103,** 127201 (2009).
34. Ijiri, Y., Schulthess, T. C., Borchers, J. A., van der Zaag, P. J. & Erwin, R. W. Perpendicular Coupling in Exchange-Biased Fe_3O_4/CoO Superlattices. *Phys. Rev, Lett.* **99,** 147201 (2007).
35. Gorodetsky, G. & Treves, D. Second-Order Susceptibility Terms in Orthorferrites at Room temperature. *Phys. Rev*. **135,** A97 (1964).
36. Cho, J. *et al.* Thickness dependence of the interfacial Dzyaloshinskii–Moriya interaction in inversion symmetry broken systems. *Nat. Commun.* **6,** 7635 (2015).
37. Chen, G. *et al.* Tailoring the chirality of magnetic domain walls by interface engineering. *Nat. Commun.* **4,** 2671 (2013).

Acknowledgements

This work was supported by the National Research Foundation of Korea (NRF) grants funded by the Ministry of Science, ICT and Future Planning (MSIP) of Korea (Bank for Quantum Electronic Materials, No. 2011-0028736 and 2013K000315).

Author Contributions

B.C. and T.H.K. conceived the project idea and planned the analytical and numerical calculations. T.H.K. performed the analytical and numerical calculations. T.H.K., P.G., S.H.H. and B.C. analyzed the data. B.C. led the work and wrote the manuscript with T.H.K. The results of the theoretical and numerical findings were discussed by all coauthors.

Additional Information

Supplementary information accompanies this paper at http://www.nature.com/srep

Competing financial interests: The authors declare no competing financial interests.

How to cite this article: Kim, T. H. *et al.* Ultrafast spin dynamics and switching via spin transfer torque in antiferromagnets with weak ferromagnetism. *Sci. Rep.* **6**, 35077; doi: 10.1038/srep35077 (2016).

This work is licensed under a Creative Commons Attribution 4.0 International License. The images or other third party material in this article are included in the article's Creative Commons license, unless indicated otherwise in the credit line; if the material is not included under the Creative Commons license, users will need to obtain permission from the license holder to reproduce the material. To view a copy of this license, visit http://creativecommons.org/licenses/by/4.0/

© The Author(s) 2016